Influence of manufacturing process on Cavitation Erosion on CoCrWMoCFeNiSiMn (Stellite 1) alloys

Vishakh Pradeep Kumar

2025-08-14 Thu

Agenda

- Introduction
- Aims
- Methodology
- Results & Discussion
- Conclusion

Introduction

Cavitation Erosion

- **What is cavitation?**
  Collapse of bubbles and the resulting high-frequency high-pressure shock waves. Caused by fluid pressure dropping to vapor pressure, which is particularly common with high fluid flow speeds [1].
- **Why does it matter?**
  Cavitation erosion leads to removal of material, crack growth, and part failure. Affects turbine blades, pump impellers, valves, stirrers, etc.

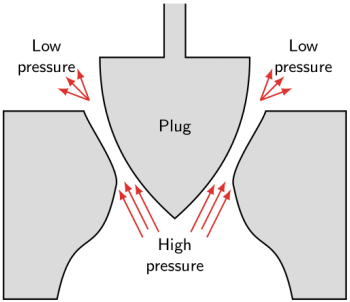

Cavitation Erosion

- **What is cavitation?**
  Collapse of bubbles and the resulting high-frequency high-pressure shock waves. Caused by fluid pressure dropping to vapor pressure, which is particularly common with high fluid flow speeds [1].
- **Why does it matter?**
  Cavitation erosion leads to removal of material, crack growth, and part failure. Affects turbine blades, pump impellers, valves, stirrers, etc.

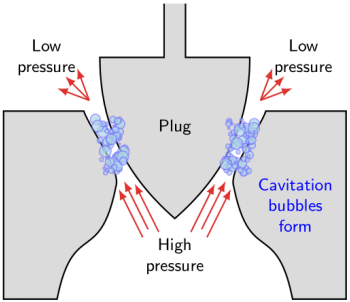

Cavitation Erosion

- **What is cavitation?**
  Collapse of bubbles and the resulting high-frequency high-pressure shock waves. Caused by fluid pressure dropping to vapor pressure, which is particularly common with high fluid flow speeds [1].
- **Why does it matter?**
  Cavitation erosion leads to removal of material, crack growth, and part failure. Affects turbine blades, pump impellers, valves, stirrers, etc.

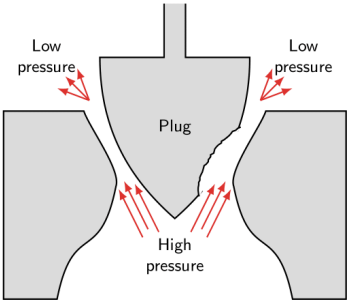

Influences on Stellite Properties

Microstructure determines Cavitation Resistance

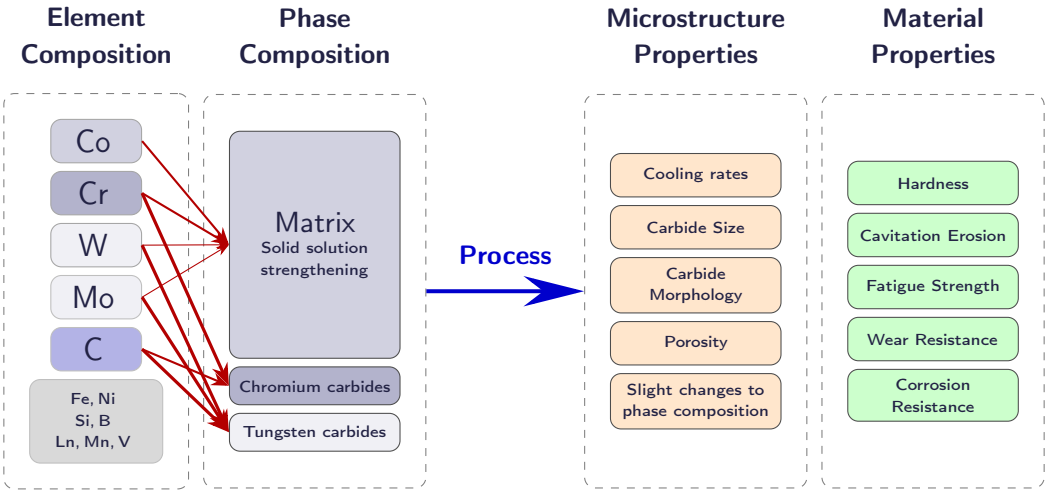

Influences on Stellite Properties

Increased Carbides, Increased Hardness, Increased Cavitation Resistance

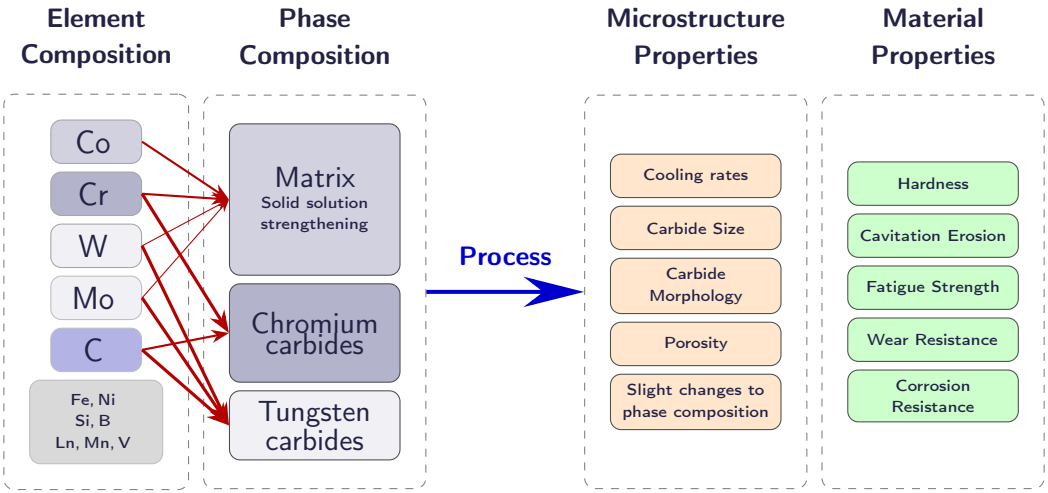

Aims

Methodology

Methodology - ASTM G32 Cavitation Erosion Testing

Naturally aerated **seawater** at room temperature.

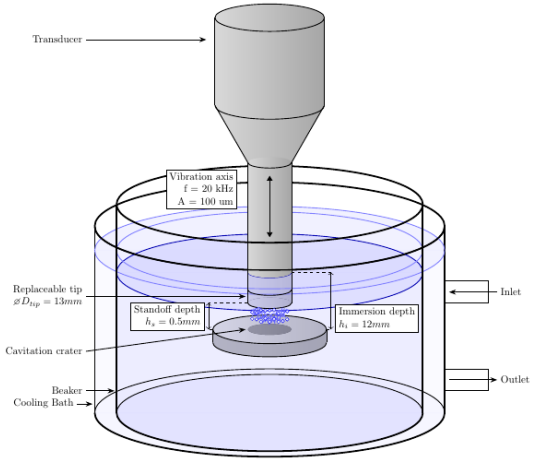

Figure 1: ASTM G32 apparatus for cavitation testing

Methodology - ASTM G32 Cavitation Erosion Testing

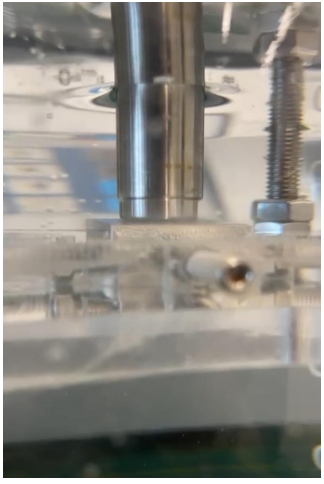

Figure 2: ASTM G32 apparatus in operation

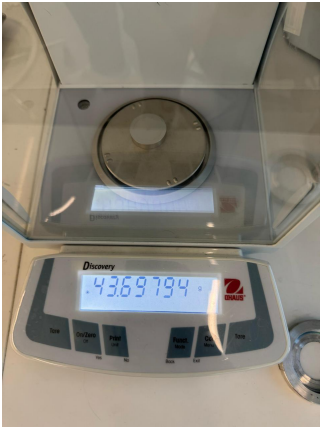

Figure 3: Analytical Balance

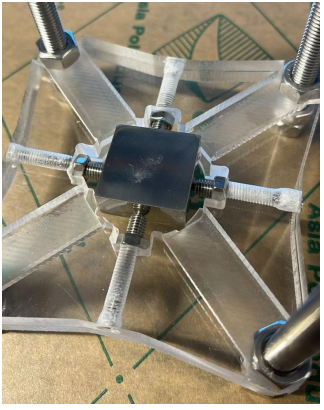

Figure 4: Custom CNC-cut sample holder

Methodology - ASTM G32 Cavitation Erosion Testing

- Seawater was vacuum filtered in order to remove algae and suspended particles
- Seawater pH was measured after calibrating pH meter with buffer solutions of pH 7 and pH 14.

Figure 5: pH Meter reading of seawater

Methodology - Electrochemical Setup

- Instrument:
  Corrtest CS310 Potentiostat
  connected to conventional three-electrode cell.
- Working Electrode (WE):
  The sample, with an exposed area of $2cm^2$.
- Reference Electrode (RE):
  Saturated Calomel Electrode (SCE).
- Counter Electrode (CE):
  Graphite plate.
- Electrolyte:
  Naturally aerated **seawater** at room temperature.

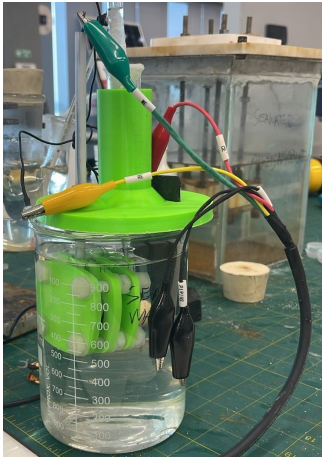

Figure 6: Three-electrode electrochemical setup

Methodology - Electrochemical Setup

Figure 7: Embedded sample after test, with corroded region

Figure 8: Top View of electrochemical setup

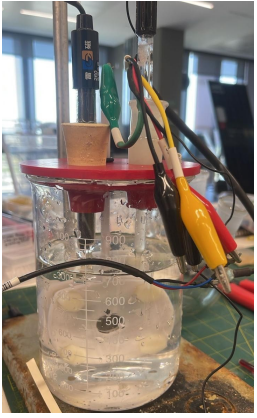

Figure 9: Initial prototype with platinum counter electrode

Methodology - Electrochemical Tests

- Open Circuit Potential (OCP)
  Before each electrochemical test, OCP was measured for one hour to ensure each sample reaches equilibrium, before EIS and LPR (explained below).
- Electrical Impedence Spectroscopy (EIS)
  The electrical response of the sample's interface with naturally aerated seawater
  - Frequency - 10^5 Hz $\rightarrow$ 10^{-1} Hz
  - Excitation voltage - **10 mV** and **20 mV**
  - Spacing - 20 per decade, logarithmic
- Linear Polarization Curve (LPR)
  The current density through the sample with an externally imposed voltage
  - Voltage - -20 mV wrt OCP $\rightarrow$ 20 mV wrt OCP
  - Scan rate - 0.1 mV/s
  - Data Acquisition rate - 10 Hz

Methodology - X-ray Diffraction (XRD)

The constituent phases were examined by X-ray diffraction

- Cu $K\alpha$ radiation ($\lambda = 1.5406\,\text{Å}$),
- Bragg-Brentano $\theta : 2\theta$,
- diffraction angle range $2\theta \in [10°, 80°]$,
- step size of $0.02°$,
- scanning time of 0.5 sec/step,
- sample rotation enabled

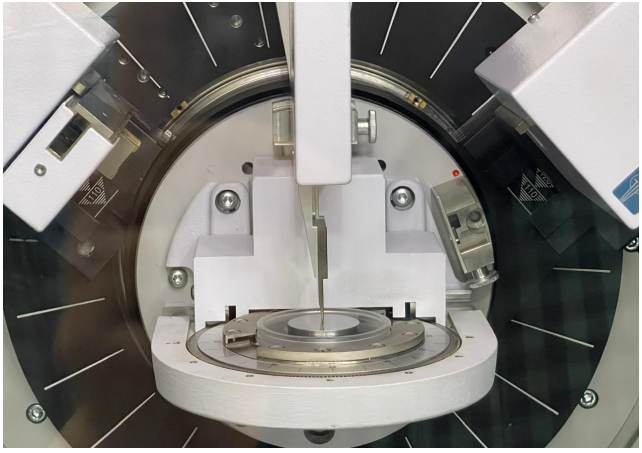

Figure 10: As-cast sample in the Bruker D8 Advance

Methodology - Optical Microscopy (OM) & Electron Microscopy (SEM)

- Optical Microscopy (OM)
  Images were taken with Amscope metallurgical optical microscope
  - eyepiece magnification 10X
  - auxiliary magnification 5X, 10X, 20X, 50X, 100X
- Scanning Electron Microscopy (SEM) Images were taken with Vega TESCAN and Oxford Instruments
  - Secondary Emission (SE)
  - Backscattered Electrons (BSE)
  - Energy Dispersive X-ray Spectroscopy (EDS)

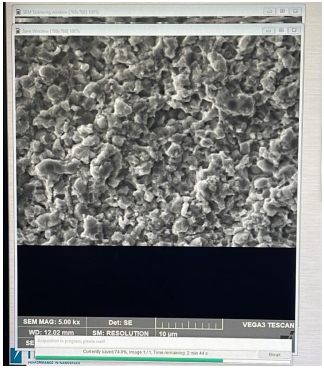

Figure 11: Screenshot of Vega TESCAN software during data acquisition of BSE image

Results & Discussion

Results - OM Images

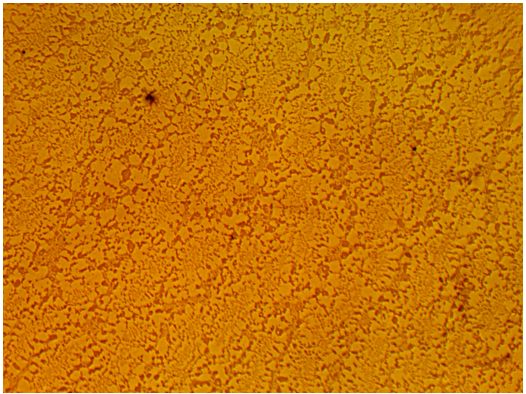

(a) As-cast Stellite 1 w/ mag 500X (specimen centre)

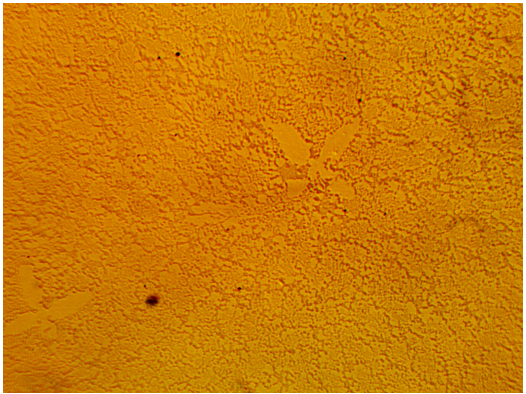

(b) HIPed Stellite 1 w/ mag 500X (specimen centre)

Figure 12: Optical Microscopy Images of as-cast and HIPed Stellite 1 specimens

Results - OM Images

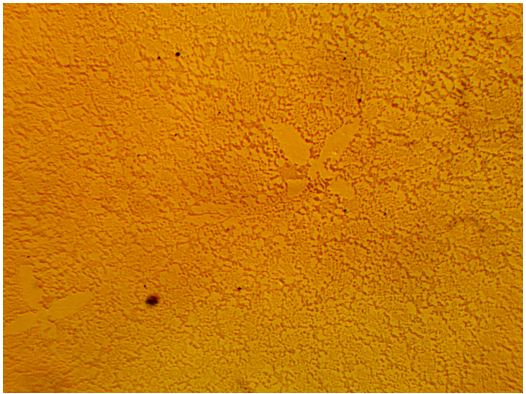

(c) As-cast Stellite 1 w/ mag 500X (specimen midway)

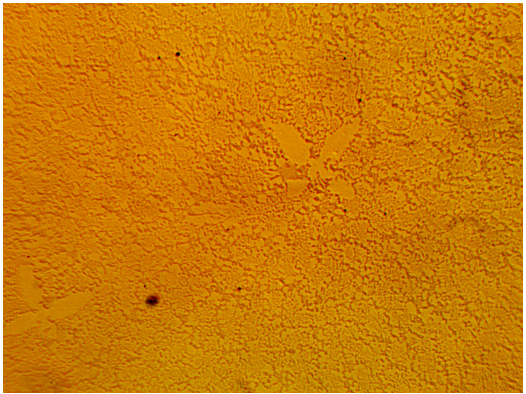

(d) HIPed Stellite 1 w/ mag 500X (specimen centre)

Figure 12: Optical Microscopy Images of as-cast and HIPed Stellite 1 specimens

Results - OM Images

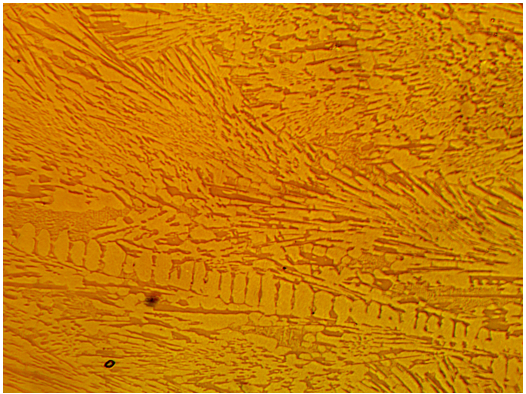

(d) As-cast Stellite 1 w/ mag 500X (specimen edge)

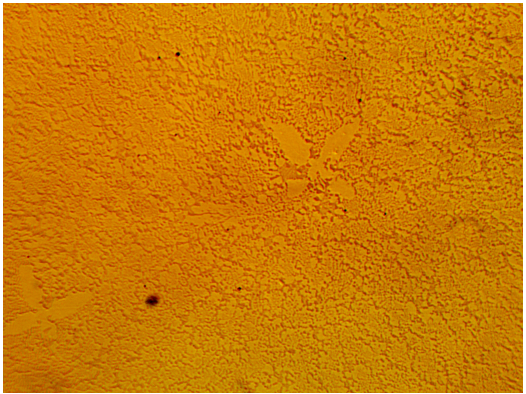

(e) HIPed Stellite 1 w/ mag 500X (specimen centre)

Figure 12: Optical Microscopy Images of as-cast and HIPed Stellite 1 specimens

Results - HIPed Stellite 1 SEM Images

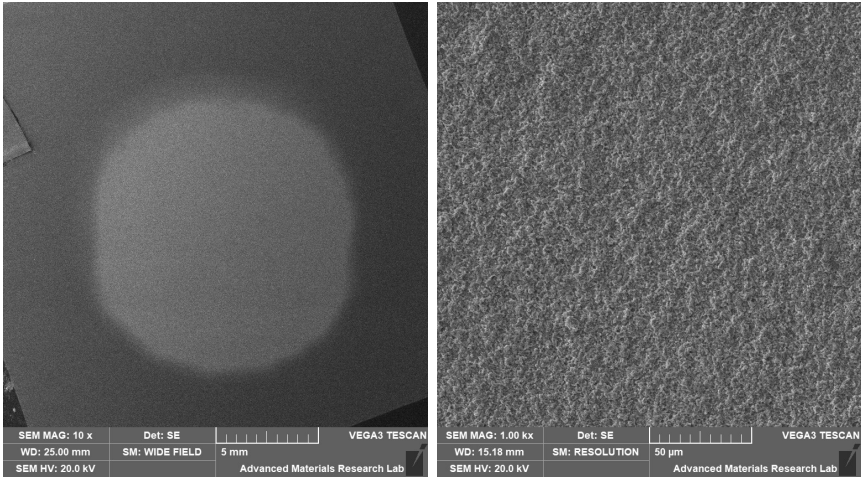

(a) SE w/ mag 10X (b) SE w/ mag 1000X

Figure 13: Eroded surface of HIPed Stellite 1

Results - HIPed Stellite 1 SEM Images

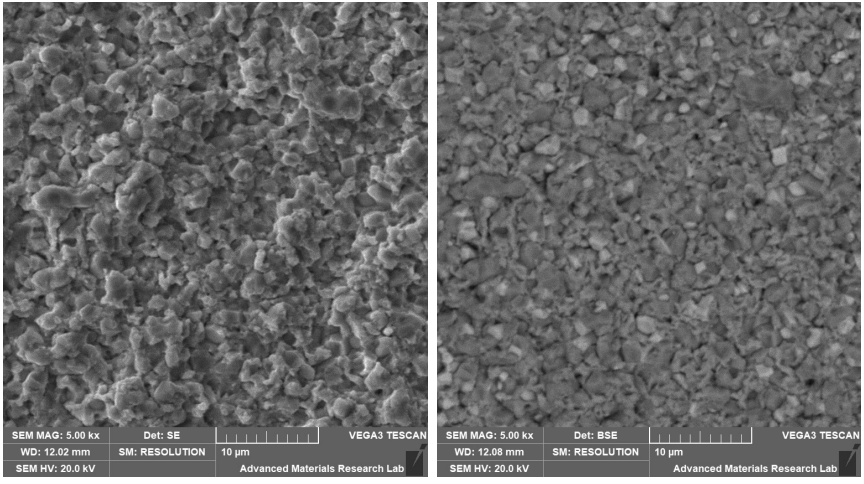

(c) SE w/ mag 5000X (d) BSE w/ mag 5000X

Figure 13: Eroded surface of HIPed Stellite 1

Results - OCP

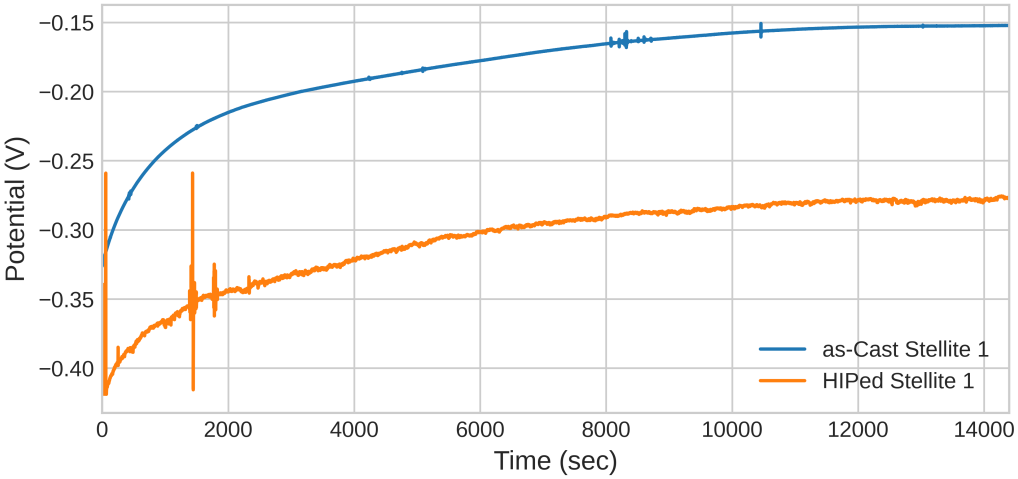

Figure 14: Open Circuit Potential (OCP) of as-Cast and HIPed Stellite 1

Results - OCP

- **OCPs shows upward trend**
  Upward (nobler) trend indicates passivation (formation of protective layer), reducing rate of corrosion.
- **HIPed S1 has lower OCP than as-cast S1**
  Lower OCP is indicative of more thermodynamically stable materials [2], [3].

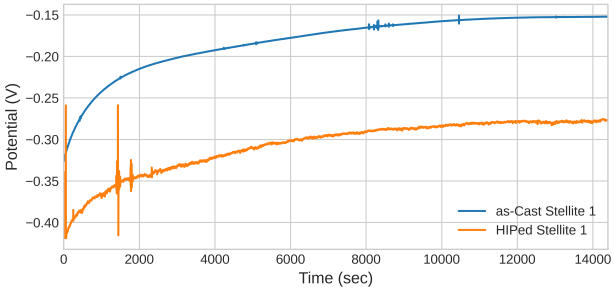

Figure 14: Open Circuit Potential (OCP) of as-Cast and HIPed Stellite 1

Results - EIS

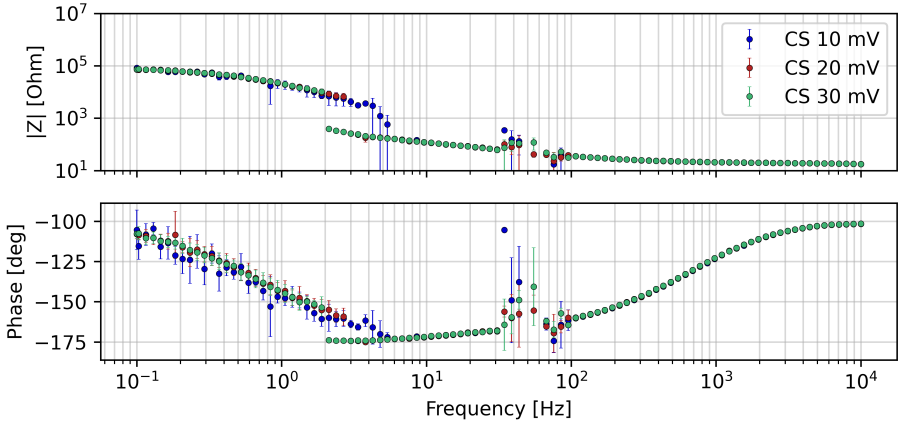

(a) EIS Bode plot of as-Cast Stellite 1

Figure 15: Comparison of EIS results with excitation frequencies 10, 20, and 30 mV

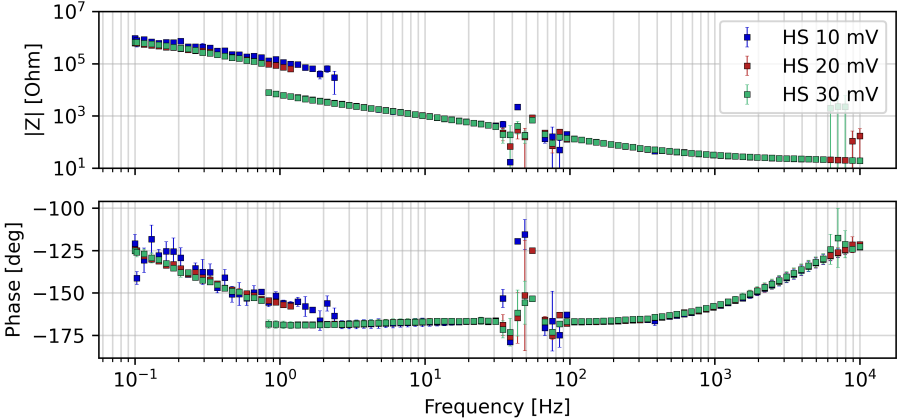

(b) EIS Bode plot of HIPed Stellite 1

Figure 15: Comparison of EIS results with excitation frequencies 10, 20, and 30 mV

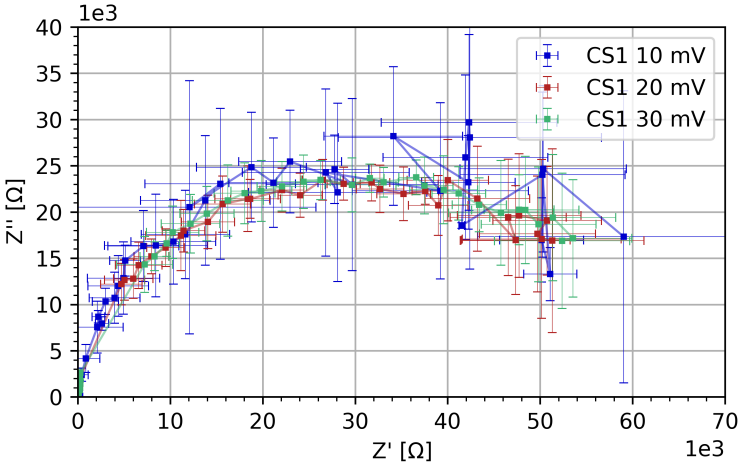

(c) EIS Nyquist plot of as-Cast Stellite 1

Figure 15: Comparison of EIS results with excitation frequencies 10, 20, and 30 mV

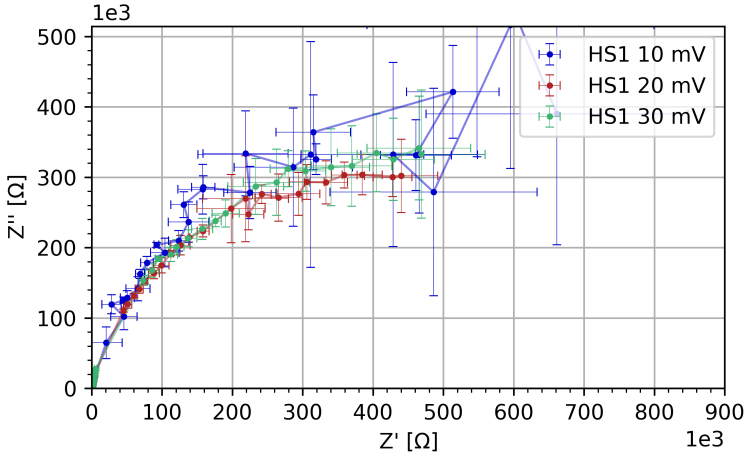

(d) EIS Nyquist plot of HIPed Stellite 1

Figure 15: Comparison of EIS results with excitation frequencies 10, 20, and 30 mV

Results - EIS

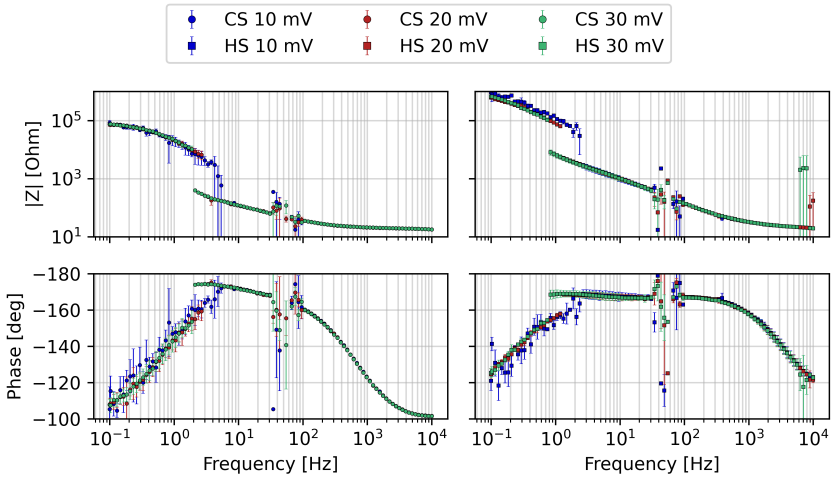

Figure 16: EIS of as-Cast Stellite 1 and HIPed Stellite 1

- **EIS is mostly independent of excitation frequency**

  The discontinuitity that appears at lower frequencies is "delayed" at higher excitation voltages, but datapoints are similar with small errorbars.

  Values taken with excitation voltage of 20mV will be used for quantitative analysis

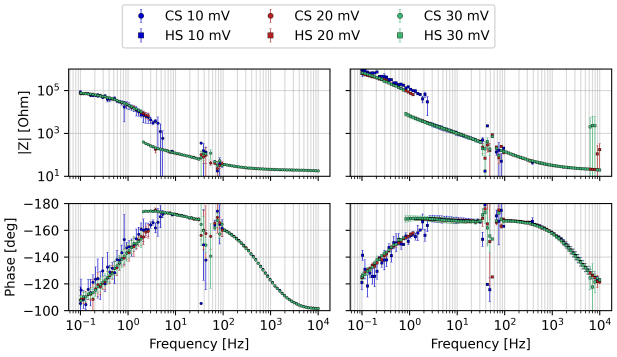

Figure 16: EIS of as-Cast Stellite 1 and HIPed Stellite 1

Results - EIS

- EIS is mostly independent of excitation frequency
- **HIPed Stellite 1 possesses greater impedence**

  Greater impedence indicates greater resistance to corrosion. Similar dependence on microstructure observed in as-cast & HIPed Stellite 6 [3], [4], [5], [6].

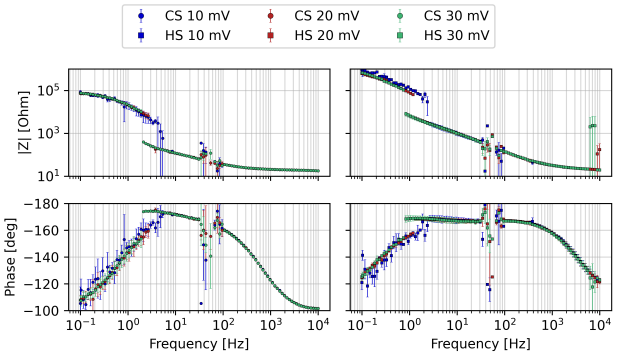

Figure 16: EIS of as-Cast Stellite 1 and HIPed Stellite 1

Results - EIS

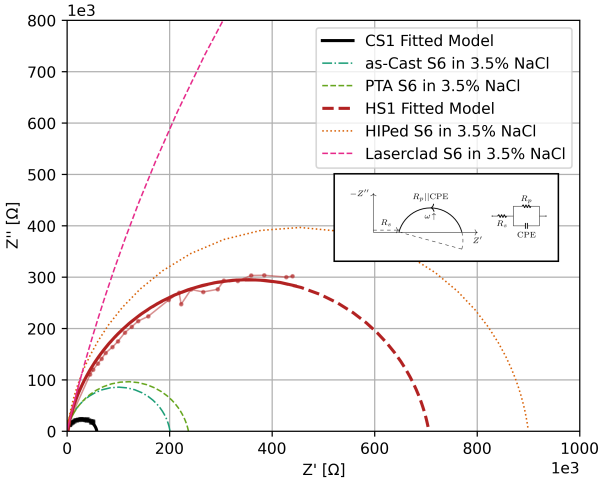

Figure 17: Equivalent Circuit fit of EIS of as-Cast Stellite 1 and HIPed Stellite 1, compared with circuit fits extracted from existing literature [3], [7], [8].

Results - EIS

- HIPed S1 shows lower resistance than HIPed S6
- as-Cast S1 shows lower resistance than as-Cast S6
- HIPing, Laserclad (high cooling rate) results in higher resistance than as-Cast, PTA (low cooling rate)
- **HIPing significantly improves corrosion resistance**

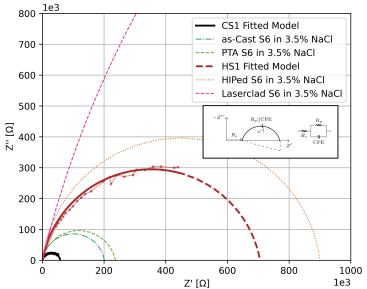

Figure 18: Equivalent Circuit fit of EIS of as-Cast Stellite 1 and HIPed Stellite 1, compared with circuit fits extracted from existing literature [3], [7], [8].

Results - Tafel

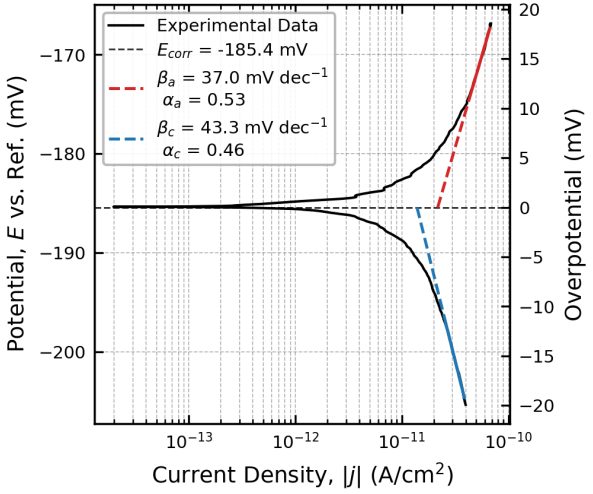

Figure 19: Tafel plot for HIPed Stellite 1

Results - Tafel

- HIPed S1 shows lower resistance than HIPed S6
- as-Cast S1 shows lower resistance than as-Cast S6
- HIPing, Laserclad (high cooling rate) results in higher resistance than as-Cast, PTA (low cooling rate)
- **HIPing significantly improves corrosion resistance**

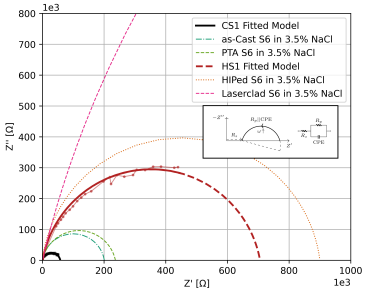

Figure 20: Equivalent Circuit fit of EIS of as-Cast Stellite 1 and HIPed Stellite 1, compared with circuit fits extracted from existing literature [3], [7], [8].

Conclusion

Effect of Casting

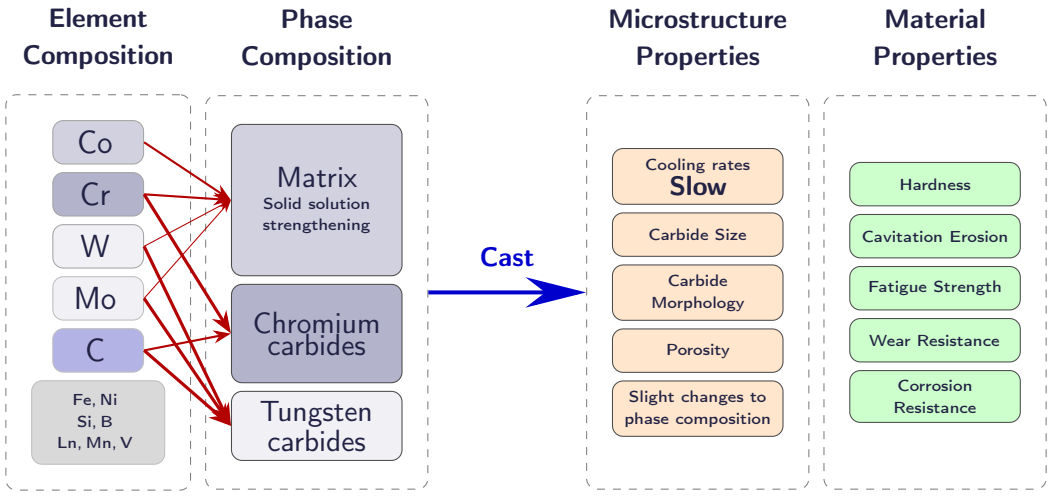

Effect of Casting

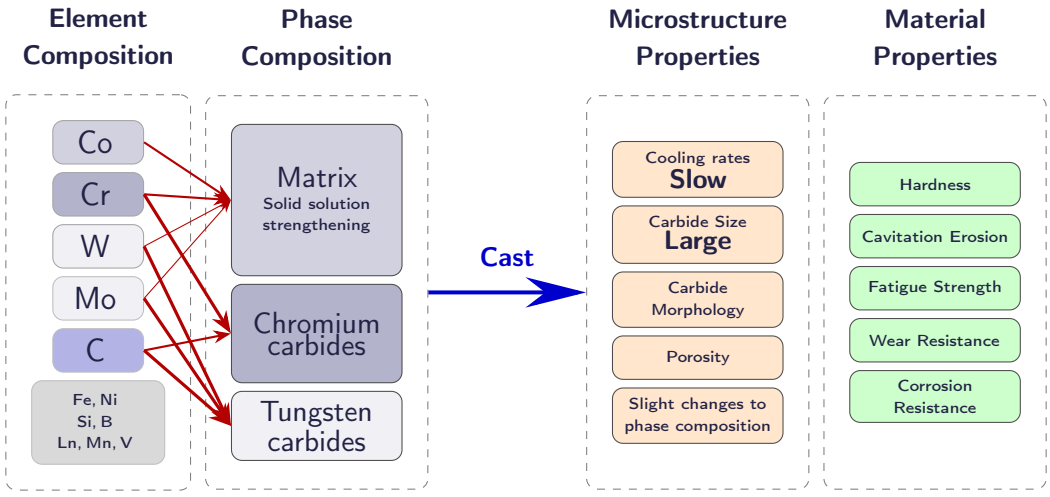

Effect of Casting

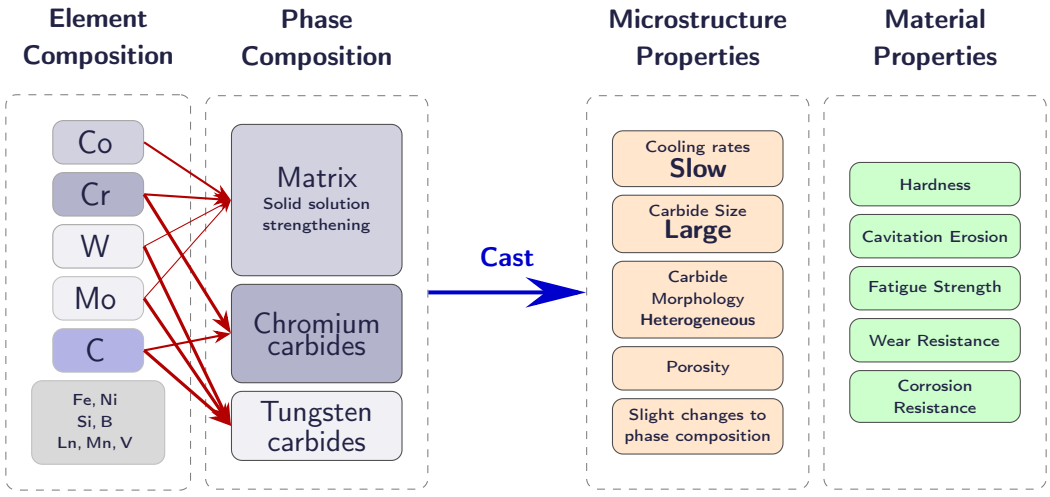

Effect of Casting

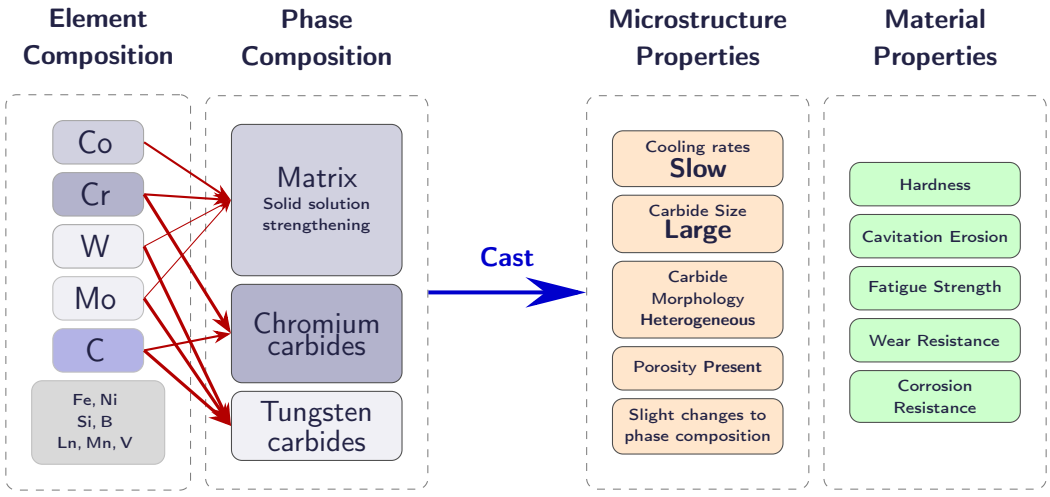

Effect of HIPing

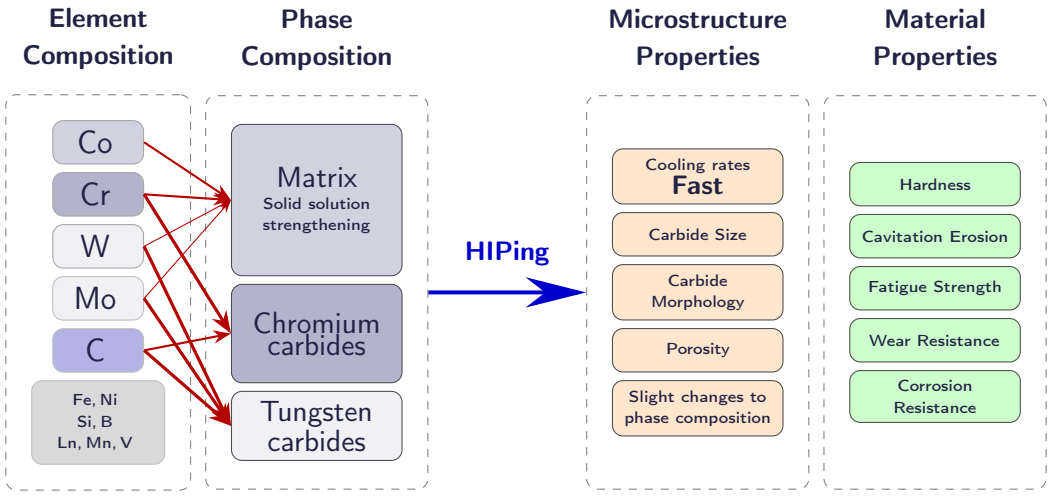

Effect of HIPing

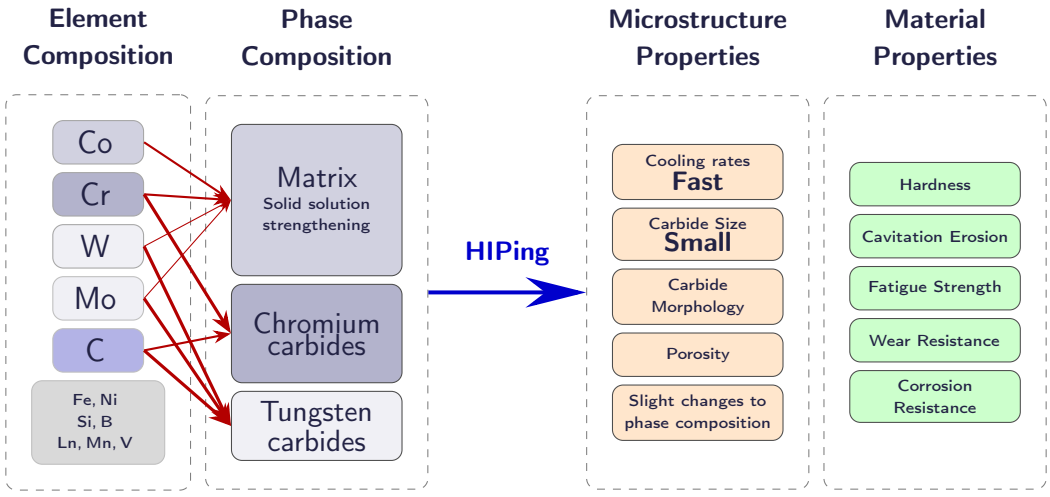

Effect of HIPing

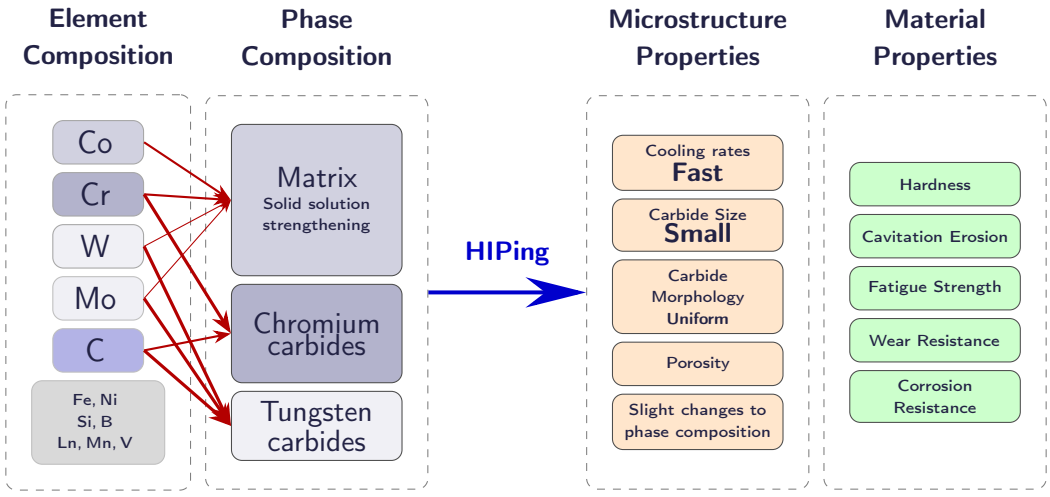

Effect of HIPing

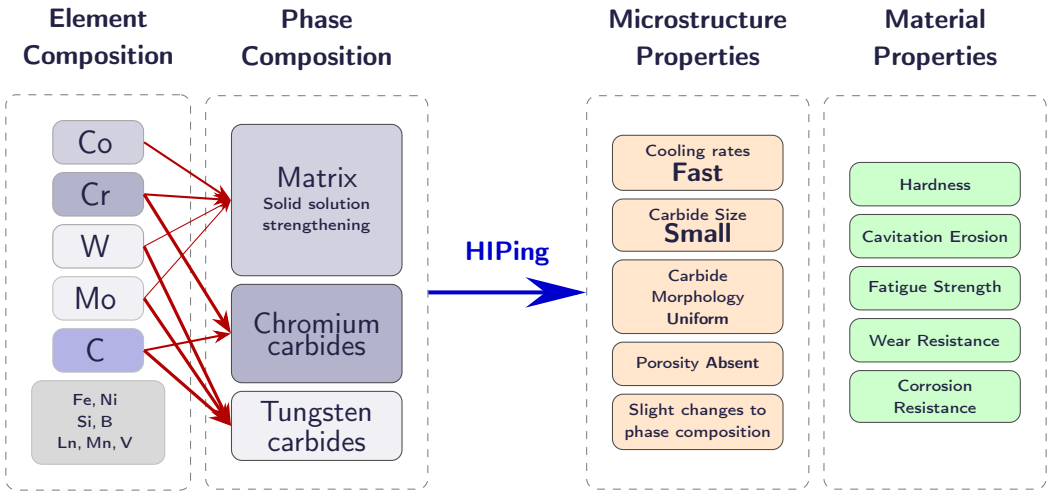

References

[1] A. K. Krella, *"Degradation and Protection of Materials from Cavitation Erosion: A Review,"* *Materials*, vol. 16, no. 5, p. 2058, Jan. 2023, ISSN: 1996-1944. DOI: 10.3390/ma16052058. Accessed: Jun. 5, 2025.

[2] N. Ogunlakin et al., *"Microstructural and Electrochemical Corrosion Characterization of a Novel 50 IN–50 Co Super Alloy Composite in 3.5wt.% NaCl Solution,"* *Journal of Materials Engineering and Performance*, Mar. 2025, ISSN: 1544-1024. DOI: 10.1007/s11665-025-10951-x. Accessed: May 27, 2025.

Bibliography ii

[3] F. Rosalbino and G. Scavino, *"Corrosion behaviour assessment of cast and HIPed Stellite 6 alloy in a chloride-containing environment,"* *Electrochimica Acta*, vol. 111, pp. 656–662, Nov. 2013, ISSN: 0013-4686. DOI: 10.1016/j.electacta.2013.08.019. Accessed: Apr. 15, 2025.

[4] U. Malayoglu and A. Neville, *"Comparing the performance of HIPed and Cast Stellite 6 alloy in liquid–solid slurries,"* *Wear*, 14th International Conference on Wear of Materials, vol. 255, no. 1, pp. 181–194, Aug. 2003, ISSN: 0043-1648. DOI: 10.1016/S0043-1648(03)00287-4. Accessed: Feb. 17, 2025.

Bibliography iii

[5] U. Malayoglu, A. Neville, and H. Lovelock, *"Assessing the kinetics and mechanisms of corrosion of cast and HIPed Stellite 6 in aqueous saline environments,"* *Corrosion Science*, vol. 47, no. 8, pp. 1911–1931, Aug. 2005, ISSN: 0010-938X. DOI: 10.1016/j.corsci.2004.09.011. Accessed: Jun. 30, 2024.

[6] A. Neville and U. Malayoglu, *"Aqueous corrosion of cobalt and its alloys,"* in *Shreir's Corrosion*, 2010, pp. 1916–1936. DOI: 10.1016/B978-044452787-5.00093-7.

[7] M. Azzi, L. Vernhes, E. Bousser, and J. E. Klemberg-Sapieha, *"Tribo Mechanical Properties of CoCr and NiWCrB Hardfacing Superalloy Coating Systems,"* in *ASME 2014 International Mechanical Engineering Congress and Exposition*, American Society of Mechanical Engineers Digital Collection, Mar. 2015. DOI: 10.1115/IMECE2014-39372. Accessed: Apr. 16, 2025.

[8] X. Wu, *"Microstructure and Performance Studies of a Novel Cobalt High Entropy Alloy,"* Master of Applied Science, Carleton University, Ottawa, Ontario, 2020. DOI: 10.22215/etd/2020-14374. Accessed: Mar. 14, 2025.